

Monte Carlo simulations of Fully Depleted CMOS pixel sensors for radiation detection applications

Original

Monte Carlo simulations of Fully Depleted CMOS pixel sensors for radiation detection applications / Ferrero, Chiara; Neubüser, Coralie; Pancheri, Lucio; Rivetti, Angelo. - ELETTRONICO. - (2023), pp. 101-104. (Intervento presentato al convegno 2023 18th Conference on Ph.D Research in Microelectronics and Electronics (PRIME) tenutosi a Valencia, Spain nel 18-21 June 2023) [10.1109/PRIME58259.2023.10161878].

Availability:

This version is available at: 11583/2981382 since: 2023-12-11T09:31:27Z

Publisher:

IEEE

Published

DOI:10.1109/PRIME58259.2023.10161878

Terms of use:

This article is made available under terms and conditions as specified in the corresponding bibliographic description in the repository

Publisher copyright

IEEE postprint/Author's Accepted Manuscript

©2023 IEEE. Personal use of this material is permitted. Permission from IEEE must be obtained for all other uses, in any current or future media, including reprinting/republishing this material for advertising or promotional purposes, creating new collecting works, for resale or lists, or reuse of any copyrighted component of this work in other works.

(Article begins on next page)

Monte Carlo simulations of Fully Depleted CMOS pixel sensors for radiation detection applications

Chiara Ferrero

Politecnico di Torino,
Dep. of Electronics Engineering
INFN - Sezione di Torino
Torino, Italy
chiara.ferrero@polito.it

Coralie Neubüser

Trento Institute for Fundamental
Physics and Applications,
INFN, Trento
Trento, Italy

Lucio Pancheri

University of Trento,
Dep. of Industrial Engineering
TIPFA-INFN, Trento
Trento, Italy

Angelo Rivetti

INFN - Sezione di Torino,
University of Torino,
Dep. of Physics
Torino, Italy

Abstract—The ARCADIA (Advanced Readout CMOS Architectures with Depleted Integrated sensor Arrays) collaboration has developed 25 μm pitch Fully Depleted Monolithic Active Pixel Sensors (MAPS) based on a modified 110 nm CMOS process in collaboration with LFoundry. This work illustrates a set of simulations performed on this detector technology, with the aim of investigating its capabilities for radiation detection applications. Three-dimensional Technology Computer Aided Design (TCAD) simulations have been performed in order to extract the electric field and electrostatic potential maps suitable to execute Monte Carlo simulations, providing high statistics of particle-sensor interaction in a reasonable computing time. The simulation flow will be described in detail and the main results will be pointed out.

Index Terms—Monolithic sensors, radiation detectors, CMOS, TCAD simulations, Monte Carlo

I. INTRODUCTION

Silicon sensors are nowadays largely employed in many applications requiring radiation detection. The two major classes of silicon pixel detectors are hybrid and monolithic detectors. In the former case, the readout electronics and the sensors are fabricated on separate chips, that are interconnected through small balls of solder: a procedure called bump bonding, that leads to high production costs. The monolithic approach, on the other hand, features an integrated front-end electronics in the same silicon volume that constitutes the sensing substrate, with great benefits in terms of material budget and production costs. Monolithic CMOS sensors are the first choice in numerous radiation detection applications, like trackers at collider experiments [1]. For example, the Inner Tracking System of the ALICE experiment at CERN is the first large-area ($\sim 10 \text{ m}^2$) silicon tracker based on the CMOS Monolithic Active Pixel Sensor (MAPS) technology [2]. Indeed, MAPS offer the intrinsic capability of providing precise 2D-information and have been demonstrated to fully satisfy the requirements posed by their application in tracking detectors of high energy physics experiments [3], as well as in other fields of research like biomedical imaging in hadron therapy radiation treatment [4]. The results presented in this work are focused on simulations of a Fully Depleted Monolithic Active Pixel Sensor (FD-MAPS), a detector technology that provides cost-effective devices for both particle tracking and timing application. It can

benefit from a low material budget, a high signal-to-noise ratio and limited diffusion of the charge carriers originated by the impinging particle [6]. A similar Monte Carlo simulation tool can be found in [7], focused on particle tracks on imaging detector arrays.

II. A FULLY DEPLETED CMOS PIXEL SENSOR

The sensor presented in this work is the Main Demonstrator pixel sensor developed by the ARCADIA (Advanced Readout CMOS Architecture with Depleted Integrated sensor Arrays) collaboration, an R&D project targeting the development of novel CMOS sensors.

The sensor design is experiment-independent and the collaboration has three main application domains that drive the development. Together with the requirements of space applications, the other two driving interests are medical applications and future colliders for high energy experiments (HEP), which require a high radiation hardness and an improved spatial resolution. The sensor performance targets very low power consumption, in the order of 20 mW cm^{-2} at 100 MHz cm^{-2} particle flux [5], fast charge collection and low cost per unit area.

A. The sensor concept

The ARCADIA sensor technology is based on a modified 110 nm CMOS process, developed in collaboration with LFoundry and is characterized by an innovative design, in which the bias voltage is provided from the backside. The process node was chosen to enable the in-pixel implementation of complex digital functions while keeping low prototyping and production costs [6].

A p+ boron-doped electrode sits at the backside of the n-substrate, constituting a pn junction at the bottom of the sensor and enabling full depletion. In this way, the sensor depletion starts from the backside of the sensor, when a sufficient negative voltage is applied and, at the same time, low supply voltages can be provided at the sensor front side. The p+ implantation is made after thinning the substrate and is activated with laser annealing. Fig. 1 shows a 3D TCAD simulation domain consisting of a single pixel with dimensions (25x25x50) μm . The collection electrodes, defined by n-type

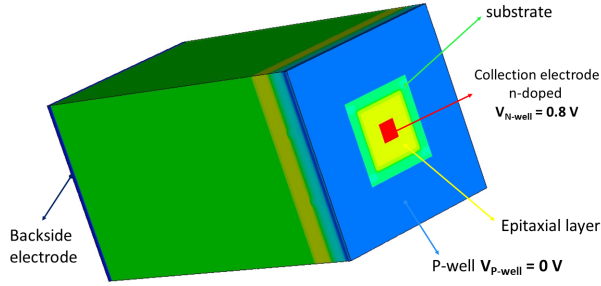


Fig. 1. TCAD single pixel simulation domain of the ARCADIA Main Demonstrator sensor. The color scale represents the doping concentration.

implantations, are located on the front side and are insulated only after the full depletion of the substrate has been reached [8]. CMOS electronics is implemented inside the n-wells (pMOSFETs) and p-wells (nMOSFETs), that are shielded by deep p-wells, preventing from charge collection competition between the sensing nodes and the n-wells hosting pMOSFETs transistors. Moreover, an additional highly n-doped epitaxial layer is located above the n-type substrate, which causes the full depletion of the substrate, including the epi-layer, to be reached at higher voltages. Its purpose is to better control the potential barrier below the deep p-well, in order to push the voltage for the onset of the punch through to higher values [9].

B. The onset of the punch-through

The maximum voltage that can be applied to the backside electrode is limited by the onset of the punch-through. This phenomenon occurs when the voltage applied to the backside electrode rises above a certain value, called V_{pt} , causing a hole current to flow between the deep p-well, sitting on the front side, and the p+ doped electrode, at the bottom of the sensor. It has been observed experimentally that this current increases exponentially and therefore the sensor operation in condition of large punch-through current has to be avoided, as it can lead to an excessive power consumption. The onset of the punch-through can be estimated from the dip in the curve of the p-well current at the top side of the sensor as a function of the voltage applied to the backside ($|V_{back}|$), as shown in Fig. 2 for three different thicknesses.

The voltage $|V_{back}|$ to be applied during TCAD simulations has been evaluated as the voltage at which a power consumption per unit of area of 10 mW/cm^2 is reached. Generally its value is slightly higher than the V_{pt} , but still in an acceptable range. Thanks to the sensor design, it is possible to supply a voltage V_{n-well} of 0.8 V at the collection nodes, to use CMOS electronics with appropriate low voltage and simultaneously to benefit from a fully depleted silicon bulk, which allows to have a strong electric field and fast signals produced by drift.

Table I contains the voltage settings used in TCAD simulation campaigns.

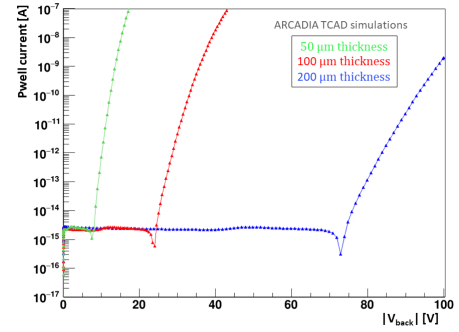


Fig. 2. Pwell current as function of backside voltage for three different thicknesses in different colors.

TABLE I
VOLTAGE SETTINGS APPLIED IN 3D TCAD SIMULATIONS

Thickness (μm)	V_n (V)	V_{pt} (V)	$ V_{back} $ (V)
50	0.8	7.5	14.5
100	0.8	24	36.5
200	0.8	73	97

III. TCAD + ALLPIX² SIMULATION CHAIN

In order to simulate devices like the CMOS sensors, advanced simulation tools are required to model their performance, study the signal formation and optimize the design of future prototypes. The studies were carried out by combining three-dimensional Technology Computer Aided Design (TCAD) and a Monte Carlo framework named Allpix² [10], implementing high statistics simulations with very precise electric field and weighting potential maps as starting points. Technology CAD simulators describe the motion of electrical carriers starting from a deterministic electron-hole generation function defined in time and space.

Allpix², on the other hand, exploits Monte Carlo methods to simulate the response of silicon sensors when crossed by a set of impinging particles interacting stochastically with the silicon lattice. For all particles crossing the active volume of the detectors, the energy loss is converted into deposited charge carriers and a list of physical processes is simulated. The peculiarity of the Allpix² framework is to combine TCAD-simulated electric fields with a Geant4 simulation of the particle interaction with matter, taking into account the stochastic nature of the initial energy deposition, with the great benefit of saving computing time [11]. Fig. 3 shows the electric field map of a 5×5 pixels simulation domain and a weighting potential map, computed to simulate induced signals on neighboring pixels [12].

Many of these properties could also be investigated by advanced TCAD transient simulations, but this approach is not practical owing to the high computing time for a single event and the high-statistics samples required. In Allpix², a simplified charge transport algorithm is used, taking as input the map calculated by the TCAD simulation of the complex field configuration within the sensor. In particular,

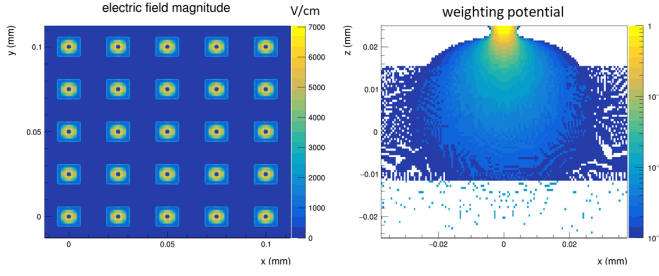


Fig. 3. Electric field map of a 5×5 simulation domain (left) and weighting potential map (right) with collection electrode in the center.

for each propagation step, the induced charge on electrode n is calculated via the Shockley-Ramo theorem as:

$$Q_n^{ind} = \int_{t_0}^{t_1} I_n^{ind} dt = q(\psi(x_1) - \psi(x_0)) \quad (1)$$

where ψ is the function describing the weighting potential displayed in Fig. 3 (right).

IV. CHARGE COLLECTION EFFICIENCY

In order to evaluate the sensor performance by varying the impinging positions of a minimum ionizing particle, a position scan has been executed on the half diagonal of the central pixel of a 5×5 matrix. It has been checked that the behaviour on the other half diagonal is symmetric. Five simulations on the half diagonal, as illustrated in Fig. 4 (left), have been performed moving the impinging position from the center to the corner of the pixel. The charge collection efficiency (CCE) has been computed as the ratio between the collected and the deposited charge. This latter has been calculated by considering that the particle deposits 80 e-h pairs per μm and, as a consequence, in the total thickness of the sensor ($50 \mu m$), 4000 e-h pairs have been deposited, which corresponds to 0.64 fC.

$$CCE(t) = \frac{Q_{coll}}{Q_{dep}} = \frac{\int_0^t I_{n-well}(t') dt'}{Q_{dep}} \quad (2)$$

with $Q_{dep} = 0.64$ fC.

The CCE has been computed from the matrix mean signals for all the simulations and in all the cases it reaches unity as shown in 4 (right), proving a complete collection of the deposited charge in the sensor. It has to be taken into account that the collection diode is located in the center of each pixel and the charges spend a longer or shorter time interval to reaching it, depending on the particle impact position. In particular, by changing the incident position from the center to the corner, the path the charges will have to travel increases and, in the same way, the drift time.

V. CLUSTER SIZE RESULTS

The following simulations have been carried out by considering μ^- with an energy of 200 MeV impinging uniformly in one pixel of a 21×21 simulation domain. After the charged

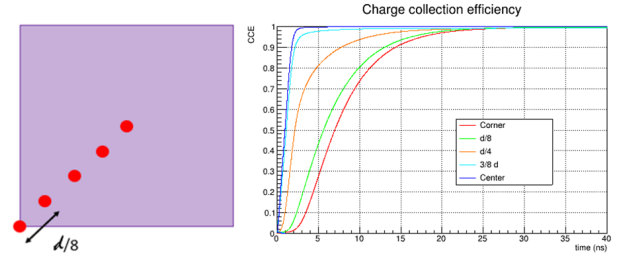


Fig. 4. Schematic visualization of the position scan executed on the half diagonal of the pixel (left) and charge collection efficiency as a function of time for the different impact positions (right)

particle crosses the active volume, it produces free charge carrier pairs by ionization, that may be shared by several pixels. A group of adjacent pixels with a signal above a certain threshold is called cluster.

The following results are focused on the cluster size evaluation, i.e the number of pixels belonging to a cluster, with a threshold set to 200 e^- , which is a reasonable value to avoid readout electronic noise [6]. Starting from a perpendicular impinging configuration and tilting then the sensor with different angles, the cluster size distributions for three sensor thicknesses of 50 μm , 100 μm and 200 μm have been investigated.

Fig. 5 shows the hitmaps, i.e the adjacent pixels of the matrix with signal above threshold, obtained with two different tilting technique: a double tilting along both x and y axes and a single tilting along the y axes only, for different angles. They represent a useful indicator to immediately visualize how the sensor tilting procedure is affecting the charge collection and the starting point to obtain the cluster size distributions.

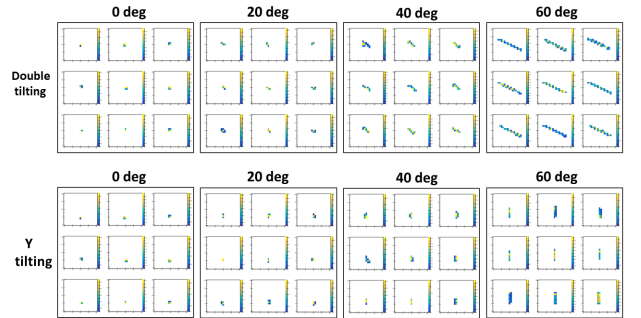


Fig. 5. Hitmaps obtained with a threshold of 200 e^- . The first row is the outcome of the double tilted sensor on both x and y axes, while the second row makes reference to y-tilted sensor. Different tilting angles are indicated in different columns.

A. Geometrical factors

First, the dependency of the cluster size from the tilting angle has been considered, as shown in Fig. 6 (left) for a sensor thickness of 100 μm . It is possible to notice the shift of the cluster size distribution to higher pixel values when the tilting increases, since the charge is shared among a higher number of pixels.

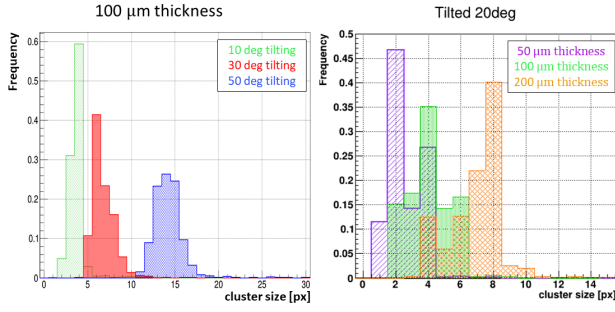


Fig. 6. Cluster size distributions for a sensor thickness of 100 μm for three different tilting angle. The plot makes reference to the double tilting procedure (left). Cluster size distributions for three different sensor thicknesses for a 20 deg double tilted sensor (right).

B. Physical sensor factors

The other dependency that has been considered in this work is the sensor thickness. Fig. 6 (right) clearly illustrates the trend of average cluster size increase with the sensor thickness for a fixed tilting angle of 20 deg. This behavior can be explained considering both the enlarged size of the particle tracks projected on the sensor surface when increasing the sensor thickness and the lateral diffusion of the charge carriers during the charge collection.

To summarize the cluster size studies conducted on the ARCADIA Main Demonstrator CMOS pixel sensor, Fig. 7 shows the trend of the cluster size as a function of the tilting angle, for a threshold set to 200 e^- . Three different thicknesses are considered and both the single and double tilting simulation results are shown. The displayed cluster size represents the average of the distribution of 1000 events for that particular configuration. The error bars represent the rms value of the cluster size distributions. From Fig. 7, one can notice that the average cluster size obtained from a perpendicular impinging configuration is a maximum of 4 pixels, while it increases with both the tilting angle and the thickness. At high tilting angles, the cluster size increase could mainly be justified by the geometrical configuration.

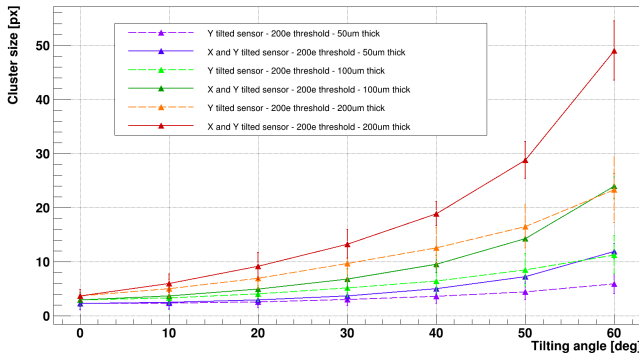


Fig. 7. Average cluster size as function of the tilting angle for three different sensor thicknesses with a fixed threshold of 200 e^- . The double tilting technique is shown in solid line, while the y-tilting is displayed in dashed line.

VI. CONCLUSIONS

The tracking performance of the Arcadia Main Demonstrator CMOS pixel sensor with 25 μm pitch designed in a technology based on a modified 110 nm CMOS process have been deeply investigated through three-dimensional TCAD simulations that, combined with Monte Carlo simulations, have provided high statistics of particle-sensor interaction. To study the tracking capabilities of the sensor, both the charge collection efficiency and the cluster size have been evaluated. The cluster size dependency from the sensor thickness and the tilting angle have been considered and two different tilting techniques have been implemented. The average cluster size for perpendicular impinging configuration is around 4 pixels, while at high tilting angles, where geometrical effects play a crucial role, a maximum of around 50 pixels is reached for the 200 μm thickness.

VII. ACKNOWLEDGEMENTS

The activity presented in this work has been carried out in the framework of the ARCADIA experiment funded by the Istituto Nazionale di Fisica Nucleare (INFN), Italy, CSN5. The simulations have been performed with the Open Computing Cluster for Advanced data Manipulation (OCCAM) cluster managed in collaboration between the University of Torino and the Sezione di Torino dell'Istituto Nazionale di Fisica Nucleare and funded by "Compagnia di San Paolo".

REFERENCES

- [1] R. Turchetta et al., "Monolithic active pixel sensors (MAPS) in a VLSI CMOS technology," Nuclear Instruments and Methods in Physics Research Section A, Vol. 501, pp. 251-259, 2003.
- [2] G. Aglieri Rinella, "The ALPIDE pixel sensor chip for the upgrade of the ALICE Inner Tracking System," Nuclear Instruments and Methods in Physics Research Section A, Vol. 845, pp. 583-587, 2017.
- [3] G. Contin, "The MAPS-based ITS Upgrade for ALICE," arXiv, 2020.
- [4] F. Baruffaldi et al., "iMPACT: An Innovative Tracker and Calorimeter for Proton Computed Tomography," in IEEE Transactions on Radiation and Plasma Medical Sciences, vol. 2, no. 4, pp. 345-352, July 2018.
- [5] C. Neubüser et al., "Sensor Design Optimization of Innovative Low-Power, Large Area FD-MAPS for HEP and Applied Science," in Frontiers in Physics, vol. 9, 2021.
- [6] L. Pancheri et al., "Fully Depleted MAPS in 110-nm CMOS Process With 100–300- μm Active Substrate," IEEE Transactions on Electron Devices, vol. 67, pp. 2393-2399, 2020.
- [7] G. Rolland et al., "STARDUST: A Code for the Simulation of Particle Tracks on Arrays of Sensitive Volumes With Substrate Diffusion Currents," in IEEE Transactions on Nuclear Science, vol. 55, no. 4, pp. 2070-2078, Aug. 2008.
- [8] L. Pancheri et al., "A 110 nm CMOS process for fully-depleted pixel sensors," in Journal of Instrumentation, vol. 14, pp. C06016-C06016, 2019.
- [9] L. De Cilladi, "Fully Depleted Monolithic Active Microstrip Sensors: TCAD Simulation Study of an Innovative Design Concept," Sensors, vol.21, 2021.
- [10] S. Spannagel et al., "Allpix2: A modular simulation framework for silicon detectors," Nuclear Instruments and Methods in Physics Research Section A, vol. 901, pp. 164-172, 2018.
- [11] D. Dannheim, "Combining TCAD and Monte Carlo methods to simulate CMOS pixel sensors with a small collection electrode using the Allpix2 framework," Nuclear Instruments and Methods in Physics Research Section A, vol. 964, 2020.
- [12] W. Riegler, "An application of extensions of the Ramo-Shockley theorem to signals in silicon sensors," Nuclear Instruments and Methods in Physics Research Section A, vol. 940, pp. 453-461, 2019.